Computational and Statistical Analysis of Gravitational Lensing OGLE Events: 2019-BLG-0227, 2019-BLG-0022

By Omri Atir & Eliran Shishportish (Instructor: Gal Birenbaum)

Abstract

This paper is about to survey the subject of gravitational microlensing and analyze two microlensing events that recorded by OGLE – Optical Gravitational Lensing Experiment. The analysis was done by applying known statistical methods and implement them by our written "Python" programming language code. The first event that we analyzed was "OGLE-2019-BLG-0227". We started with simplifying the mathematical model of the event and fit a parabolic function for specific part of the data. Then we fitted the full data to a more complexed nonlinear model. We searched for two of the characterizing parameters of the model (2D) that will yield minimum of χ^2-statistical parameter. Then we enabled freedom for four characterizing parameters (4D) and used the same method. Eventually we explored another event: "OGLE-2019-BLG-0022" and used the more complexed four parameters fitting to test our full developed statistical methods implemented by our code. Our results showed identical quality fit parameter - $\chi^2_{reduced}$ for both 2D and 4D fittings, but lower N_σ values for 2D fit with theoretical OGLE values than 4D fit with OGLE values. The differences are small, and we think that the preferable fitting method depends on available computational resources, which is the factor that limits the resolution, and to the prior information that is available about the microlensing event.

2) Introduction

Gravitational lensing is a phenomenon that occurs when the path of light is bent by the gravitational field of massive objects, such as stars, galaxies, or clusters of galaxies. While Albert Einstein made initial calculations on the subject in 1912, it was Orest Khvolson (1924) and Frantisek Link (1936) who are generally acknowledged as the first to discuss this effect in published works. Nevertheless, Einstein's association with gravitational lensing is widely recognized, as he published an article on the topic in 1936 [1]. This effect was confirmed by observation of twin quasar in 1979. The twin quasar was a quasar[1] that appeared as two images because of gravitational lensing caused by the galaxy YGKOW G1 that is located directly between earth and the quasar [2].

Theoretical Background

1.1 Types of lensing: Weak & Strong Lensing

We can divide the lensing phenomenon into two types, weak and strong. These two types are categorized by their differences in noticeable optical effects, and their magnification strength. Strong lensing produces observable by telescope effects, such as the formation of multiple images, arcs, or even complete Einstein rings (discussed in section 1.3). Strong lensing cause significant magnification of the source light, even by tens of percents. On the other hand, weak lensing characterizes by faint change in the magnification, only few percents, of the source, and there is no creation of multiple images.

1.2 Lensing Geometry

The geometry abstraction of gravitational lensing is depicted in figure 1. The source denoted as S, is placed in an angle β from the optical axis, emits light ray that deflected by angle $\hat{\alpha}$, by the gravity of the massive object that behave as a lens. After the deflection the ray reaches to the observer – "O". The image that the observer see –"I" is separated by angle α from the real source, and by angle θ from the optical axis. The closest distance that the light approaches the mass, is denoted as ξ and is also called the impact parameter. The angle α is called

[1] Quasar – is an extremely luminous stellar object.

reduced deflection angle and related to $\hat{\alpha}$ by the relation:

$$(1)\ \ \alpha = \frac{D_{ds}}{D_s}\hat{\alpha}$$

Where D_{ds},D_s is the distances between the source and the lens, observer respectively. It is important to note that all the angles are small and approximated by small angles approximation.

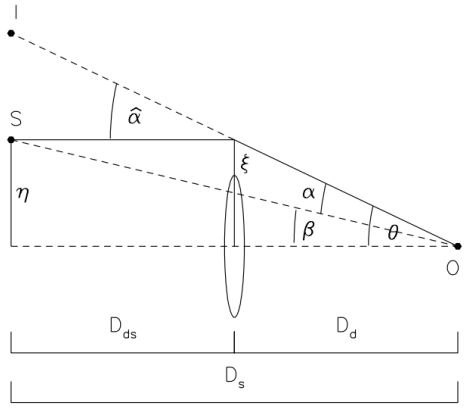

Figure (1) – gravitational lensing geometry. The angle between the optical axis of the lens and the image is θ. The angle between the source and the image is α, and between the source and the optical axis is β. The deviation angle between the undeflected ray and the image is $\hat{\alpha}$. The distance between observer and the projected of the source on the optical axis is D_s, and between the lens is D_d. The closest distance that the ray passing near the lens is ξ and the distance between the source and the optical axis is η. Image taken from "Lectures on Gravitational Lensing" [8].

From direct look at the geometry, we can didact that:

$$(2)\ \ \beta = \theta - \alpha$$

This equation is called the lens equation.

The angle $\hat{\alpha}$ can be derived in another way using our knowledge about general relativity. A calculation (which we won't detail about) of a photon trajectory in the Schwarzschild metric, under some limiting conditions of the parameters: ξ (the impact parameter) and assuming the lens is a point mass M, sitting on the optical axis at distance D_d from the observer, will result the relation [7]:

$$(3)\ \ \hat{\alpha} = \frac{4GM}{c^2\xi}$$

Where G is gravitational constant, c is the speed of light. Combining eq. 1 and eq. 3, and the geometric relation: $\xi = \theta D_d$ (D_d is the distance between the observer and the lens) we get:

$$(4)\ \ \alpha(\theta) = \frac{4\pi GMD_{ds}}{c^2 D_s D_d \theta}$$

This relation helps us to develop the natural scale of the phenomenon which called the Einstein angle.

1.3 Einstein Ring Einstein angle and multiple images

A special case of strong lensing is happening when the source, the lens and the observer is all set on the optical axis of the lens. In this case the angle $\beta = 0$, and we witness the phenomenon of Einstein ring. The ring that we witness, is caused by symmetrical deflection of the emitted rays from the source which will appear deform as a ring surrounding the lensing object. The ring has and angular radius called θ_E and we can calculate it by applying eq. 4 in the lens equation – eq. 2 and set β to zero. This will define a quadratic equation where θ is the unknown parameter, and solving it would yield:

$$(5)\ \ \theta_E = \sqrt{\frac{4MGD_{ds}}{c^2 D_d D_s}}$$

this angle is the natural scale the characterize the phenomenon of gravitational lensing.

Now that we define θ_E, we will treat the case where $\beta \neq 0$. In this case, we can write the lens equation as:

$$(6)\ \ \beta = \theta - \frac{\theta_E^2}{\theta}$$

This equation has two solutions:

$$(7)\ \ \theta_{\pm} = \frac{1}{2}\left[\beta \pm (\beta^2 + 4\theta_E^2)^{\frac{1}{2}}\right]$$

Thus, there will be always two lensed images for a point – mass lens when $\beta \neq 0$. These solutions have opposite signs; hence they will appear on both sides of the optical axis. This is something that we could expect because when looking at fig. 1, we could draw a different ray emitted from the source, passing through the bottom side of the lens and focus in "O" point by the lens. The continuation of the ray by the observer will present the second expected image.

1.4 Gravitational Microlensing

Microlensing categorized as strong lensing, in a sense that the phenomenon does create multiple images, but they cannot be angularly separated by any telescope. The lensing objects may be stars in our galaxy and the background source is a star in remote galaxy or one in our galaxy. The property that testifies microlensing is change in the magnification which implies change in the amplification, i.e., the source image will appear brighter. We can quantify the magnification, μ :

$$(8)\ \ \mu(t) = \frac{u^2 + 2}{u\sqrt{u^2 + 4}}$$

Where $u = \frac{\beta}{\theta_E}$. In case of microlensing events, we observe a continuous change in the brightness of the source. Looking at eq. 7 we see that the time changing quantity that defines the magnification is the angle β. Thus, we can infer that when microlensing event happens, that is because of relative motion of the source, the lens, and the observer. This motion modeled and presented in the figure below.

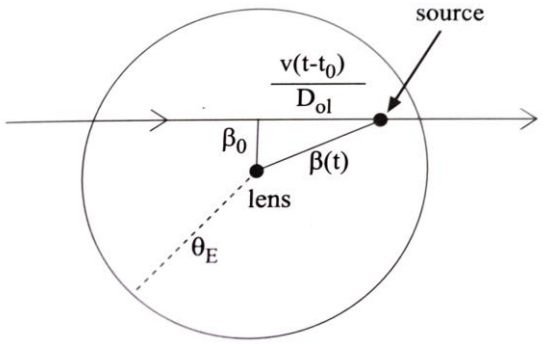

Figure (2) – relative movement of source-lens-observer positions. lens as a point-mass in the center surrounded by angular radius θ_E. Source moving at arrow direction in velocity v, and angle $\beta(t)$ between inside the page direction and lens source line. $D_{ol} = D_d$ is the distance observer-lens. Image was taken from [8].

The figure present direct look from observer point of view, where the into the page direction is the direction of the optical axis. The relative movement presented is a relative motion of the source at velocity v in the lens's plane. We define β_0 as the angle when the source is closest to the lens and T_0 is its matching time. D_{ol} is the observer-lens distance. Then by Pythagorean theorem:

$$(9)\ \beta(t) = \beta_0^2 + \frac{v^2(t-T_0)^2}{D_{ol}}$$

Translated to:

$$(10)\ u(t) = \left[u_{min}^2 + \frac{(t-T_0)^2}{\tau^2}\right]^{\frac{1}{2}}$$

Where $u_{min} = \frac{\beta_0}{\theta_E}$ is the minimal normalized angle. and $\tau = \frac{\theta_E D_{ol}}{v}$ is the characteristic time of microlensing event. To connect $u(t)$ and measured intensity we need to consider the blending parameter f_{bl}. This parameter represents the light interference portion that come from other factors other than the source that we want to explore. Such that:

$$(11)\ f_{bl} = \frac{I_{source}}{I_{total}}$$

When all the intensity comes only from the source $f_{bl} = 1$ and when there is outside light interference $1 > f_{bl} > 0$. Finally, the connection between the intensity I and the magnification (which contains dependent in $u(t)$) is:

$$(12)\ I(t) = I_*\mu(t)f_{bl} - I_*(1-f_{bl})$$

Where I_* is the intensity of the source without any gravitational microlensing i.e., $t, \beta, u \to \infty$.

1.5 Uses of Gravitational Lensing

Gravitational lensing has proven to be a valuable tool in various areas of astrophysics and cosmology. For example, microlensing techniques have been used to search for planets outside the solar system, to constrain the nature of dark matter, constrain the binary star population and constrain the structure of the Milky Way's disc [1]. Weak lensing can be used to map the distribution of galaxies on the largest scale of the universe and map the mass of the lens [3]. Strong lensing can be used to discover distant radio galaxies and inferring cosmological constants [4]. To explore microlensing events, a Polish astronomical project called OGLE – Optical Gravitational Lensing Experiment was established in 1992. This project based at University of Warsaw, runs a long-term sky survey (from its begging until now) that tracks microlensing events. In the paper we chose to analyze two microlensing events "2019-BLG-0227, 2019-BLG-0022". BLG stands for galactic bulge meaning that the source and the lens are in Milkey way galaxy. We chose the first event such that there is more than twenty points of data near the peak of the intensity. This would help us to fit a simple model to the phenomenon as described in section 2.2.2. Then, we used numerical and statistical tools for the analysis of the events, that are detailed about in the methods section.

2) Experimental Methods

2.1 Arrange the data:

The data from OGLE presents magnitude vs. time information. To convert magnitude to intensity we used this formula:

$$(13)\ \frac{I}{I_*} = \tilde{I} = 10^{-\frac{1}{2.5}(m(t)-m_*)}$$

Where, $m(t)$ is the measured magnitude and m_* is the magnitude when the source is not lensed. To find m_* we focused on the data where the curve m(t) starts to flat and did average over those values. Its error, Δm_*, was taken as simple variance error: $\frac{\sigma}{\sqrt{N}}$

where σ is m_* standard deviation and N is the number of data points taken for average.

From there, we could extract the error of $\tilde{I}$ by indirect error calculation:

$$(14)\quad \Delta I = 10^{-\frac{1}{2.5}(m(t)-m_*)} \cdot \frac{\log(10)}{2.5}\sqrt{\Delta m^2 + \Delta m_*^2}$$

Where Δm was taken from OGLE data.

The time data units were given in heliocentric Julian day units (HJD). To present the time scale in more readable way, we found the data point with maximum intensity, and its matching time. All other data points time were subtracted by this time. So, we got time scale in days, both positive and negative, in relation to the maximum point time.

2.2 Statistical Analysis:

in this section, we will explain the statistical fundamental methods which we used to analyze and estimate the reliability of our results.

2.2.1 Least Squares and χ^2 Minimization [5]

The least square method is the process of finding the best fitting curve for a set of data points by reduction the sum of the squares of the offsets of the points from the curve, normalized by each data point uncertainty (error) squared. We call this sum χ^2 and we can write it as:

$$(15)\quad \chi^2 = \sum_{i=1}^{N}\left(\frac{y_i - f(x_i, \boldsymbol{a})}{\sigma_i}\right)^2$$

Such that, N is the number of data points that we have, x_i is the data of the independent variable – we assuming it has no error. y_i is the data of the dependent variable, we assume it was measured with corresponding error - σ_i. $f(x_i, \boldsymbol{a})$ is the fitted function that we want to find, this function, describing our mathematical initial modeling, and depends on coefficient vector $\boldsymbol{a} = (a_1, a_2, \dots, a_M)$. As said above, the goal is to minimize χ^2. To do so, we will solve M equations that satisfy: $\left\{\frac{d\chi^2}{da_i}\right\}_{i=1,\dots,M}$. solving them, will guarantee minimum of χ^2 and we can extract the $\boldsymbol{a}$ and its error.

We can also define the degrees of freedom - ν (DOF) of the fit:

$$(16)\quad \nu = N - M$$

Where N is the number of data points used in the fit and M is the number of the free parameters of the fitting function. From there, we can define $\chi^2_{reduced}$ as an absolute quality fit parameter, which we want to be closest to 1.

$$(17)\quad \chi^2_{reduced} = \frac{\chi^2}{\nu}$$

2.2.2 Linear Fitting using Least Squares [5]

First, we wanted to build a simplified model that will simplify the relation in eq.12. we cut the data of the microlensing event around its peak intensity. Within this section, the data looks to obey parabolical relation. We preformed χ^2 minimization (detailed in the 2.2.1 section) to parabolical fitting function:

$$(18)\quad f(x) = a_0 + a_1 x + a_2 x^2$$

Where f represents normalized intensity - $\tilde{I}$ and x represents time. We used preliminary analysis written in "R. Barlow, Statistics" book [5], which provide information about least squares method for linear fitting functions, using matrices, to extract (a_0, a_1, a_2). For second degree polynomial function, we define **C** matrix:

$$\boldsymbol{C} = \begin{pmatrix} 1 & x_1 & x_1^2 \\ 1 & x_2 & x_2^2 \\ 1 & x_3 & x_3^2 \\ \vdots & \vdots & \vdots \end{pmatrix}$$

Where x_i represents time data. We also define $\boldsymbol{V}$ matrix as diagonal matrix that contains in the diagonal the corresponding error of $f(x_i)$:

$$\boldsymbol{V} = \begin{pmatrix} \Delta y_1 & 0 & \dots \\ 0 & \Delta y_2 & \cdots \\ \vdots & \vdots & \ddots \end{pmatrix}$$

And the vector $\boldsymbol{a}$ and is error will be extracted according to the formula:

$$(19)\quad \boldsymbol{a} = \left(\widetilde{\boldsymbol{C}}\boldsymbol{V}^{-1}\boldsymbol{C}\right)^{-1}\widetilde{\boldsymbol{C}}\boldsymbol{V}^{-1}$$

$$(20)\quad \Delta\boldsymbol{a} = diag(\boldsymbol{C}\boldsymbol{V}^{-1}\boldsymbol{C})^{-1}$$

Where $\boldsymbol{y} = f(\boldsymbol{x})$.

After extracting coefficient vector and its error, we could extract matched physical values:

$$(21)\quad T_0 = -\frac{a_1}{2a_2} \pm \sqrt{\left(\frac{\Delta a_1}{2a_2}\right)^2 + \left(\frac{\Delta a_2 a_1}{2a_2^2}\right)^2}$$

$$(22)\quad \tilde{I}_{max} = a_0 - \frac{a_1^2}{4a_2} \pm \sqrt{\Delta a_0^2 + \left(\frac{2a_1\Delta a_1}{4a_2}\right)^2 + \left(\frac{a_1^2\Delta a_2}{4a_2^2}\right)^2}$$

Where, T_0 is the time of the peak of the curve, and $\tilde{I}_{max}$ is its matching intensity value. Combining eq. 8, 10 and 12, assuming $f_{bl} = 1$, we see that $\tilde{I}_{max}$ is received when $t = T_0$ and $u = u_{min}$. Therefore, we

can extract u_{min} and its error (showed in appendix 1), by inversing the connection in eq. 7:

$$(23)\ u_{min} = \sqrt{-2 + \frac{2}{\sqrt{1-(\tilde{I}_{max})^{-2}}}}$$

To ensure that the errors of u_{min} are in reasonable range, we used the following method.

2.2.3 Bootstrap Method [6]

The bootstrap method is a simulation technique that is often used when it is not possible to repeat the experiment or we don't know enough about the underlying process, or the nature of our measurement's errors. The method uses the actual data set, with its N data points, and select randomly N data points within the set. The selection is done with replacements of the data after choosing. Because of the replacements, we do not get back the original set, instead we get in typical $\approx 37\%$ of duplicated original points. After we get those points, we repeat any statistical analysis that we choose, based on the new generated data set. During results analysis, we made histograms presenting the bootstrap results and fitted gaussians function to them so we can extract the histogram standard deviation and mean. We compared the mean- $x_{bootstrap}$ with the matching fit parameter result - x_{fit} and calculated the relative difference:

$$(24)\ relative\ difference = \frac{|x_{fit} - x_{bootstrap}|}{x_{fit}}$$

And checked if the standard deviation is in the same order of magnitude as fit parameter error.

2.2.4 2D Nonlinear Fitting

In this part, we wanted to fit all the data using the full formulas that describe the model. The full model described by eq. 8,10,12. Combining them together and applying $f_{bl} = 1$, we got the fitting function:

$$(25)\ f(x) = \frac{x^2+2}{x\sqrt{x^2+4}}$$

Such that $f(x)$ is $\tilde{I}$ and x is $u(t)$. Therefore, this fitting was clearly not linear fitting. To do so, we created 2D mesh-grid that each square in the grid presented a pair of (u_{min}, T_0) values. The τ parameter was set according to the theoretical value on appendix 2. For each pair we calculated χ^2 values according to eq.15 and found the minimal χ^2 and its matching pair. We repeated this process, each time with higher resolution grid or shifted grid limits, each time trying to get 1% χ^2_{min} improvement. After we found optimal values, we normalized the grid by subtracting all χ^2 values by χ^2_{min}. From the grid that we got, we plotted 2D contours that presents equal χ^2 lines. These contours tell us about our confidence level of our extracted parameters. That means, that we have p percent chance (see table 1) that the actual parameters are inside the contour. Each contour defined by $\Delta\chi^2$ distance in comparison to χ^2_{min}. The detailed connection between confidence levels, $\Delta\chi^2$ and ν – the degrees is freedom (the number of free parameters) are presented in the table below:

$\Delta\chi^2$ as a Function of Confidence Level and Degrees of Freedom						
	ν					
p	1	2	3	4	5	6
68.3%	1.00	2.30	3.53	4.72	5.89	7.04
90%	2.71	4.61	6.25	7.78	9.24	10.6
95.4%	4.00	6.17	8.02	9.70	11.3	12.8
99%	6.63	9.21	11.3	13.3	15.1	16.8
99.73%	9.00	11.8	14.2	16.3	18.2	20.1
99.99%	15.1	18.4	21.1	23.5	25.7	27.8

Table (1) –Confidence levels- p as functions of degrees of freedom of our free parameters space and $\Delta\chi^2$ contours. Taken from "Numerical Recipes in C" book [6].

The p percent levels are similar to confidence levels in normal distribution, such that the first one represents one standard deviation - σ from χ^2_{min}, the second 2σ and so on. In addition, to extract parameters errors, we can set one parameter that we found as constant and find where the other parameter intersects the $\Delta\chi^2 = 1$ contour.

$$(26)\ \chi^2\left(y_{2D} \pm \frac{\Delta y^+}{\Delta y^-}\right) = \chi^2 + 1\ \ ,(\nu = 1)$$

such that y stands for the one free parameter. Note that the error is not necessarily symmetrical.

2.2.5 4D Nonlinear Fitting

this part we did the same process as in the previous part, but instead of 2D fit, we built 4D mesh-grid where each cell contains the parameters: $(u_{min}, T_0, \tau, f_{bl})$. We set boundaries for each parameter in the grid and calculated for each cell χ^2 value. We found minimal χ^2 is this 4D space and fixed the fit parameters that corresponded with this specific cell. We did the same iteration process with the same stop criteria to achieve better results. We used eq. 26 to find parameters errors. With the parameters we plotted full data nonlinear fitting. And lastly, we plotted a corner plot to observe the correlation between each pair of free parameters presented on 2D while other two parameters are fixed according to their optimal values.

2.2.6 OGLE 2019-BLG-0022 Analysis

To test the tools and methods we developed for microlensing event analysis, we repeated on previous section (2.2.5) process with another microlensing event – OGLE 2019-BLG-0022. This event has f_{bl} parameter different than 1. We compared the optimal set of parameters with OGLE theoretical parameters and plotted corner plot with confidence levels.

3) Results

3.1 OGLE 2019-BLG-0227 event analysis

linear approximation

according to section 2.2.2 we sampled the data near the peak intensity of the curve. The optimal parameters (presented in eq. 18) that we got are:

Parameter	Value	Relative error
a_0	$1.4036 \pm 6.6 \cdot 10^{-3}$	0.47%
$a_1 \left[\frac{1}{day}\right]$	$-9 \cdot 10^{-5} \pm 2.9 \cdot 10^{-4}$	320%
$a_2 \left[\frac{1}{day^2}\right]$	$-2.25 \cdot 10^{-4} \pm 2.4 \cdot 10^{-5}$	11%

Table (2) – fitting parameters for parabolic approximation. OGLE 2019-BLG-0227 event.

Using them we extracted the values of T_0, u_{min} using eq. 21-23:

Parameter	Value	Relative error
$T_0\ [HJD]$	2458599.71 ± 0.63	not relevant
u_{min}	0.9220 ± 0.0074	0.76%
χ^2	33	-
$\chi^2_{reduced}$	0.62	-

Table (3) –extracted values from parabolic approximation.

$\chi^2_{reduced}$ is close to its ideal value of one. We plotted parabolic approximation for the data. The fit and the residuals shown in figure 3 below.

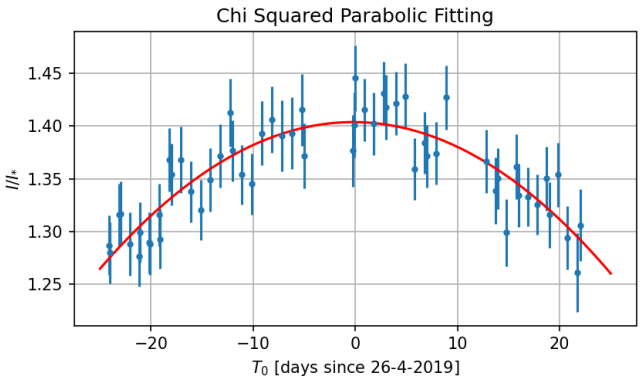

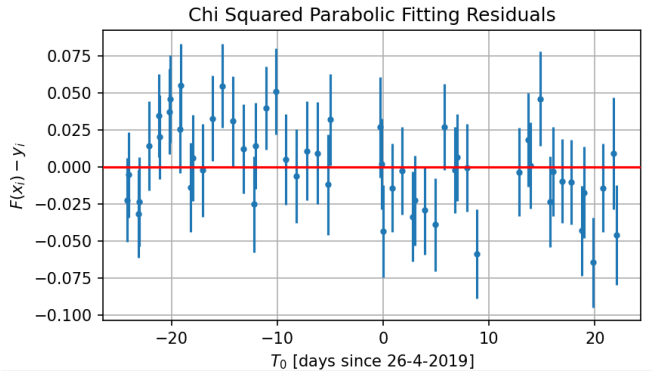

Figure (3) – parabolic fitting and its residuals graph, using χ^2 minimization. OGLE 2019-BLG-0227 event.

Bootstrap simulation for linear approximation

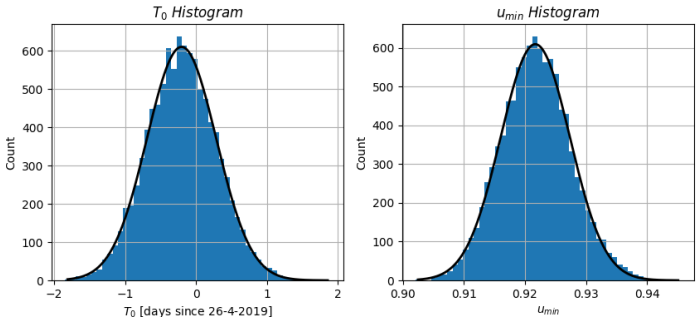

Figure (4) –bootstrap simulation histogram with 10,000 data sets and gaussian fit according to the histogram.

Which yield the following parameters:

Parameter using bootstrap	Value	Relative error
$T_0\ [HJD]$	2458599.70 ± 0.49	not relevant
u_{min}	0.9217 ± 0.0057	0.62%

Table (4) –bootstrap simulation values according to parabolic approximation.

We calculated the relative difference (by eq. 24) between bootstrap results and parabolic fit results:

	T_0	u_{min}
Relative difference	0	$3.2 \cdot 10^{-4}$

Table (5) –relative difference between fit values and bootstrap mean values.

We see that the relative difference of u_{min} is one order smaller than both fit and bootstrap u_{min} errors. That indicates good bootstrap result. Also, we see that both u_{min} and T_0 bootstrap errors are in the same order as u_{min}^{fit} , T_0^{fit} errors. That indicates reasonable fit error results.

To summarize linear fit results and compare them by N_σ test we present table 6.

	$T_0\ [HJD]$	u_{min}
parabolic fit	2458599.71 ± 0.63	0.9220 ± 0.0074
bootstrap	2458599.70 ± 0.49	0.9217 ± 0.0057

OGLE values	2458599.86 ± 0.25	0.919 ± 0.003
N_σ: *fit vs bootstrap*	0.013	0.032
N_σ: *fit vs OGLE*	0.22	0.38

Table (6) –comparison between values of u_{min}, T_0 achieved by parabolic fitting and bootstrap method, along with comparison to their theoretical values at OGLE.

Overall, we see that all N_σ values are in desired range of under 3, and our statistical analysis worked well.

2D Nonlinear fit

We created 2D grid of (u_{min}, T_0) points, while $f_{bl} = 1$ and $\tau = 42.826$ [days] were constants according to their theoretical values on OGLE. From the grid we could extract the point where χ^2 is minimal. The result is shown in table 7.

Parameter	Value	Relative error
T_0 $[HJD]$	$2458599.69\ ^{+0.52}_{-0.48}$	not relevant
u_{min}	$0.9215\ ^{+0.0054}_{-0.0052}$	0.57%
χ^2	350	-
$\chi^2_{reduced}$	0.60	-

Table (7) – optimal parameters found by minimizing χ^2 on two-dimensional parameters grid (u_{min}, T_0).

Taking the parameters that we found and applying them in eq. 24, we plotted the nonlinear fit and the residuals graph.

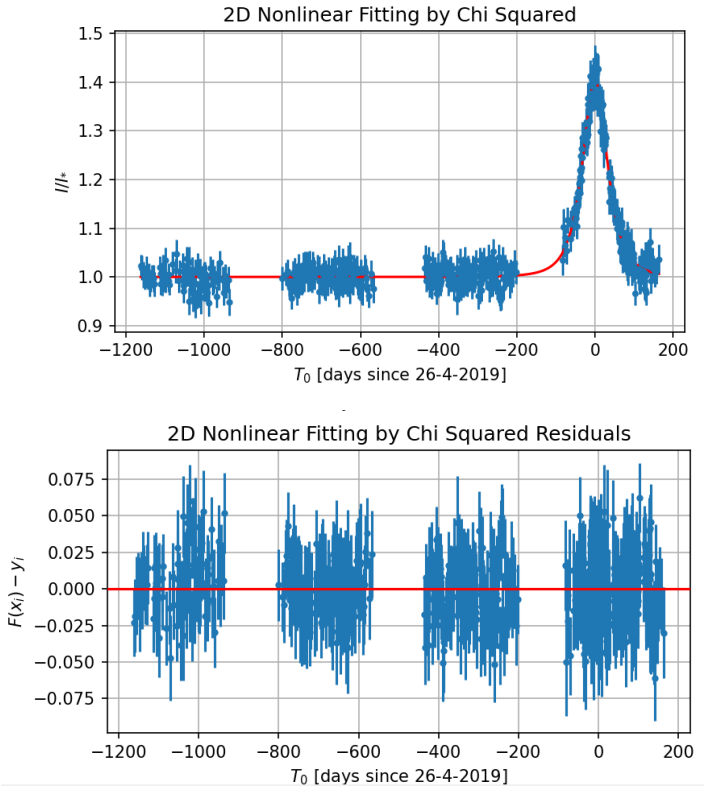

Figure (5) –2D nonlinear fitting and its residuals graph. $f_{bl} = 1$ and τ equals to its OGLE value. OGLE 2019-BLG-0227 event.

Overall, the fit seems to match the full set of data. The residuals graph showing random scattering of points along the fitting graph. From N_σ calculations on table 8 we can see that the fitting 2D parameters are close to their theoretical values. Also, $\chi^2_{reduced}$ is close enough to 1. By those fit quality parameters, we can say that the fit was a success. We plotted confidence levels (detailed how in section 2.2.4) and extracted fit parameters errors. Those errors are in the same order of theoretical values errors. The 2D contour is shown in fig. 6, and we can see that it is in very slightly tilted elliptical shape. Which means there is almost no correlation between $\{u_{min}, T_0\}$.

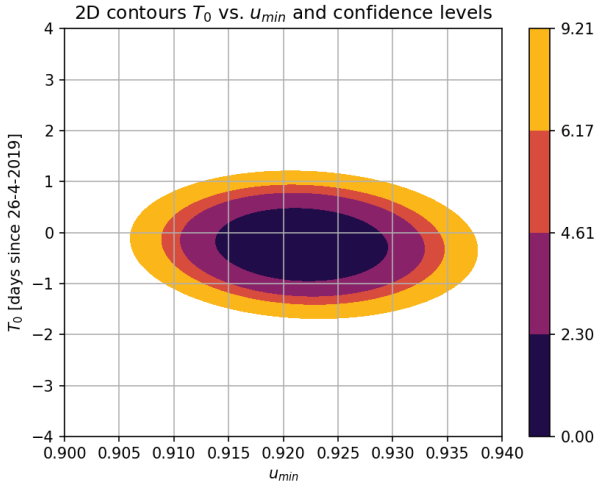

Figure (6) –Confidence levels for 2D nonlinear fitting. The figure shows 2D parameter space of u_{min} vs. T_0.

Bootstrap simulation for 2D nonlinear fit

We preformed bootstrap simulation as in parabolic fit, but now it was for 2D nonlinear fit method. This process demanded long computational time, so we simulated only 1,000 data sets and found matching fitting parameters. The histograms are shown in fig. 7 below.

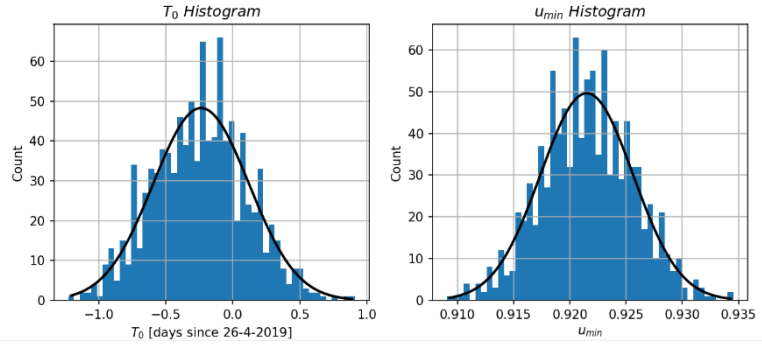

Figure (7) –bootstrap simulation histogram with 1,000 data sets and gaussian fit according to the histogram. Based on 2D nonlinear fitting.

The discrete histogram bars do not create smooth gaussian shape. We assume that is because the bootstrap repetitions were not enough to create smooth shape but enough to fit them gaussian functions. From the fitting we got the following parameters:

Parameter using bootstrap	Value	Relative error
T_0 $[HJD]$	2458599.68 ± 0.36	not relevant
u_{min}	0.9215 ± 0.0041	0.44%

Table (8) –bootstrap simulation values according to 2D nonlinear fitting.

We can see that the errors of the bootstrap parameters that we got are in the same order as fit and theoretical values. The relative difference of u_{min} is very small. N_σ values of all 2D comparisons are all lower than 1. These facts further approve 2D fit results.

	T_0 $[HJD]$	u_{min}
N_σ: $2D\ fit\ vs\ bootstrap$	0.016	0.0030
N_σ: $2D\ fit\ vs\ OGLE$	0.30	0.41
Relative difference bootstrap vs. fit	0	$2.2 \cdot 10^{-5}$

Table (9) – comparison by N_σ of fit, bootstrap and OGLE theoretical values. Also, relative difference between bootstrap and fit values.

4D Nonlinear fit

We preformed nonlinear fit with four free parameters set: $\{u_{min}, T_0, \tau, f_{bl}\}$,further detailed in section 2.2.5. we got the following results.

Parameter	4D fit	OGLE Value	N_σ
T_0 $[HJD]$	$2458599.58\ ^{+0.54}_{-0.48}$	2458599.86 ± 0.25	0.47
u_{min}	$0.9144\ ^{+0.0050}_{-0.0060}$	0.919 ± 0.003	0.74
τ	43.15 ± 0.57	42.83 ± 0.39	0.46
f_{bl}	0.983 ± 0.012	1	1.4
χ^2	351		
$\chi^2_{reduced}$	0.60		

Table (10) – optimal parameters found by minimizing χ^2 on four-dimensional parameters grid $(u_{min}, T_0, \tau, f_{bl})$. OGLE 2019-BLG-0227 event.

With them we plotted a full data nonlinear fit:

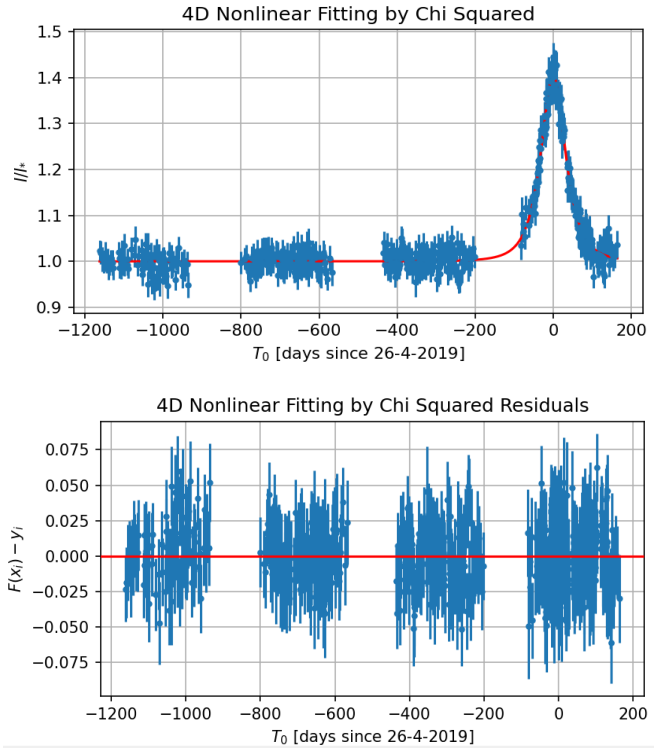

Figure (8) – fit and residuals graphs for 4D fitting. OGLE 2019-BLG-0227 event.

Overall, the fit seems to match the data. The residuals graph shows random scattering around the fit. All N_σ values are in the desired range. there are no major differences between fit and theoretical values. $\chi^2_{reduced}$ is identical to 2D result.

we build corner plot (fig. 9) to observe the correlations between different parameters. We see that there is strong correlation between $\{f_{bl}, u_{min}\}$ pair, such that increasing/decreasing one of them will force to increase/decrease the other one to maintain optimal fit.

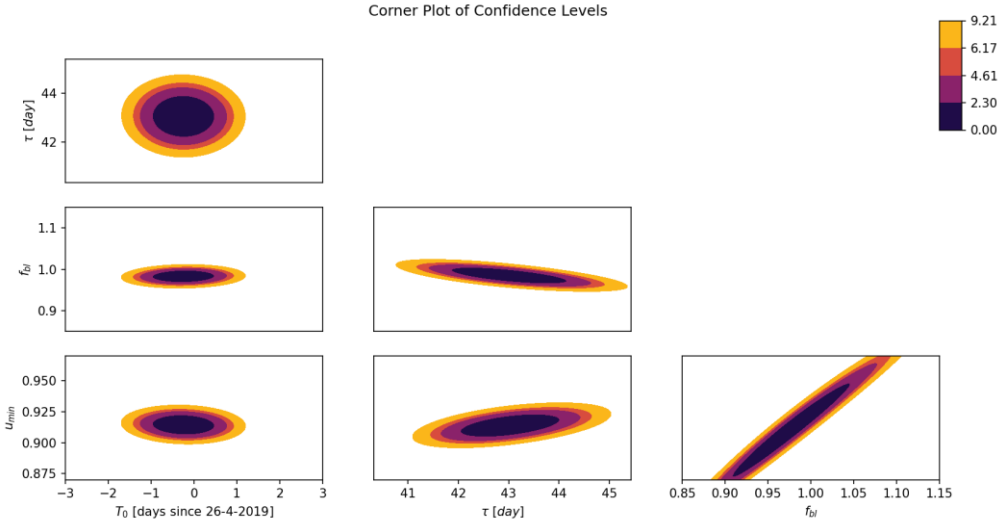

Figure (9) – 4D fitting corner plot present correlations between pairs of parameters while other two free parameters are the optimal fit values. OGLE 2019-BLG-0227 event.

The reason for this is that both f_{bl} and u_{min} affect the same property of the fitting, which is the peak intensity. We can also see small correlations between $\{f_{bl}, \tau\}$ and $\{\tau, u_{min}\}$.

3.2 OGLE 2019-BLG-0022 event analysis

We repeated the 4D fit process as in previous section, but we analyzed different microlensing event with $f_{bl} \neq 1$. We got the following results:

Parameter	4D fit	OGLE Value	N_σ
T_0 $[HJD]$	2458574.427 ± 0.073	2458574.580 ± 0.03	1.9
u_{min}	0.3861 ± 0.0010	0.396 ± 0.007	1.4
τ	$48.01\ ^{+0.16}_{-0.14}$	47.12 ± 0.58	1.5
f_{bl}	$0.5132\ ^{+0.0015}_{-0.0012}$	0.530 ± 0.014	1.2
χ^2	2700		
$\chi^2_{reduced}$	0.69		

Table (11) – optimal parameters found by minimizing χ^2 on four-dimensional parameters grid $(u_{min}, T_0, \tau, f_{bl})$. OGLE 2019-BLG-0022 event.

All parameters are close to their theoretical OGLE values by N_σ value. In addition, all errors are in the same order as OGLE values. $\chi^2_{reduced}$ is close to one, even better than we got analyzing the previous event. This indicates good fit results as we can see it visually in fig. 10.

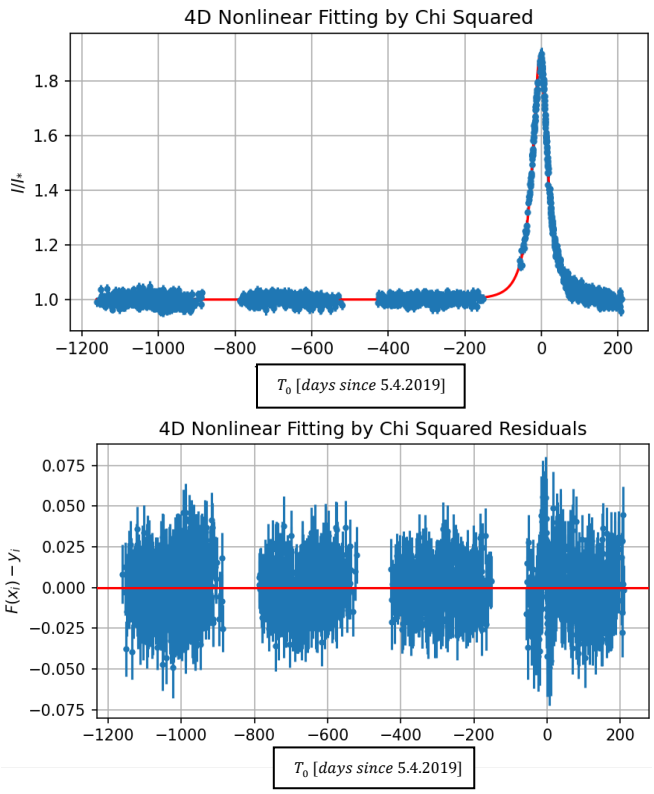

Figure (10) – fit and residuals graphs for 4D fitting. OGLE 2019-BLG-0227 event.

The residuals graph shows random scattering and no special trend. The corner plot on fig. 11 shows the same $\{f_{bl}, u_{min}\}$ correlation discussed in previous section. And other pairs relatively small correlations. Overall, we can say that the tools we developed for microlensing events analysis were successful.

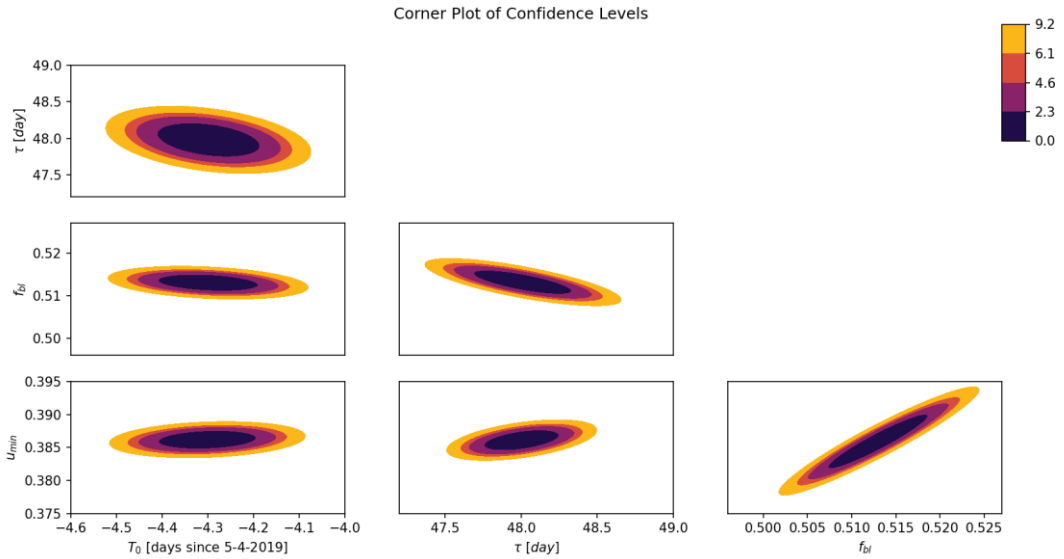

Figure (11) – 4D fitting corner plot present correlations between pairs of parameters while other two free parameters are the optimal fit values. OGLE 2019-BLG-0022 event.

4) Discussion and conclusions

In this section, we conclude our study by presenting the outcomes and conclusions of our comprehensive analysis of two microlensing events: OGLE 2019-BLG-0227 and OGLE 2019-BLG-0022, using various statistical methodologies applied in our "Python" code. First, we started with an initial parabolic approximation fit. Second, a more intricate two-parameter nonlinear fit was executed across the entire dataset, maintaining the $\{\tau, fbl\}$ parameters as constants, which yielded a successful fit. The goodness of these fits was further validated through the implementation of the bootstrap method, revealing closely aligned values and errors compared to those derived from the fitting process. In addition, those fit parameters are close to OGLE theoretical values and further approve the fit.

For deeper analysis, we wanted to give more flexibility to the nonlinear fit. To do so, we wrote an additional code of four-parameter fit applied to the complete dataset. This fit demonstrated success in deriving fitting parameters that characterize the event. We plotted a corner plot presenting pair parameters correlation. From the plot we saw that there is strong correlation between $\{u_{min}, f_{bl}\}$ pair. This result is not surprising because this pair affect the same property of event: the maximum intensity.

We found that the quality fit parameter - $\chi^2_{reduced}$ was identical on both 2D and 4D fittings. We think that is because of our computational memory limitations. The grid resolution of 2D fitting was far greater then 4D fit grid. Considering we used OGLE theoretical values and assuming it was calculated with better precision and better computational resources, we did not see improvement of $\chi^2_{reduced}$ between 2D and 4D fittings.

In order to test our algorithm, we analyzed an additional microlensing event characterized by $f_{bl} \neq 1$. Our algorithm exhibited good fittings as well, with N_σ lower than 3 and even closer to one $\chi^2_{reduced}$.

In summation, we find our outcomes to be highly satisfactory, with each of the presented fits effectively describing the microlensing phenomenon.

5) References

[1] Wikipedia. Gravitational Lens url: https://en.wikipedia.org/wiki/Gravitational_lens

[2] Wikipedia. Twin Quasar url: https://en.wikipedia.org/wiki/Twin_Quasar

[3] https://pweb.cfa.harvard.edu/research/topic/gravitational-lensing#:~:text=Weak%20lensing%20is%20also%20a,daylight%20filtering%20through%20a%20forest.

[4] https://pweb.cfa.harvard.edu/news/discovering-distant-radio-galaxies-gravitational-lensing

[5] Barlow, Roger J. *Statistics: a guide to the use of statistical methods in the physical sciences*. Vol. 29. John Wiley & Sons, 1993.

[6] Teukolsky, Saul A., Brian P. Flannery, W. H. Press, and W. T. Vetterling. "Numerical recipes in C." *SMR* 693, no. 1 (1992): 59-70.

[7] Maoz, Dan. *Astrophysics in a Nutshell*. Vol. 16. Princeton university press, 2016.

[8] Narayan, Ramesh, and Matthias Bartelmann. "Lectures on gravitational lensing." *arXiv preprint astro-ph/9606001* (1996).

6) Appendix

[1] u_{min} error using linear fit.

$$\Delta u_{min} = \frac{\Delta \tilde{I}_{max}}{u_{min} \tilde{I}^2_{max} \sqrt{\tilde{I}^2_{max} - 1}}$$

[2] OGLE-2019-BLG-0227 theoretical values

T_{max}	2458599.859 ± 0.252 (2019-04-26.36 UT)
tau	42.826 ± 0.387
u_{min}	0.919 ± 0.003
A_{max}	1.406 ± 0.003
D_{mag}	0.370 ± 0.001
f_{bl}	1.000 ± 0.000
I_{bl}	17.700 ± 0.001
I_0	17.700 ± 0.001

[3] OGLE-2019-BLG-0022 theoretical values

T_{max}	2458574.580 ± 0.030 (2019-04-01.08 UT)
tau	47.120 ± 0.578
u_{min}	0.396 ± 0.007
A_{max}	2.673 ± 0.045
D_{mag}	1.068 ± 0.000
f_{bl}	0.530 ± 0.014
I_{bl}	16.664 ± 0.000
I_0	17.352 ± 0.028